Published in final edited form as:
Nat Struct Mol Biol. 2014 November ; 21(11): 955–961. doi:10.1038/nsmb.2902.

Crosstalking noncoding RNAs contribute to cell-specific neurodegeneration in SCA7

Jennifer Y. Tan[1,2,°], **Keith W. Vance**[#1,2], **Miguel A. Varela**[#2], **Tamara Sirey**[1,2], **Lauren M. Watson**[2,3], **Helen J. Curtis**[2], **Martina Marinello**[4,5,6,7,8], **Sandro Alves**[4,5,6,7,8], **Bruno Steinkraus**[9], **Sarah Cooper**[10], **Tatyana Nesterova**[10], **Neil Brockdorff**[10], **Tudor Fulga**[9], **Alexis Brice**[4,5,6,7,8], **Annie Sittler**[4,5,6,7], **Peter L. Oliver**[1,2], **Matthew J. Wood**[2,3], **Chris P. Ponting**[1,2,§], and **Ana C. Marques**[1,2,§,°]

[1]MRC Functional Genomics Unit, University of Oxford, Oxford, UK

[2]University of Oxford, Department of Physiology, Anatomy and Genetics, Oxford, United Kingdom

[3]University of Cape Town, Division of Human Genetics, Cape Town, South Africa

[4]Centre de Recherche de l'Institut du Cerveau et de la Moëlle épinière, Hôpital de la Pitié-Salpêtrière, Paris, France

[5]Université Pierre et Marie Curie-Paris 6, Paris, France

[6]Inserm, U 975, Paris, France

[7]CNRS, UMR 7225, Paris, France

[8]Département de Génétique et Cytogénétique, APHP, GH Pitié-Salpêtrière, Paris, France

[9]Weatherall Institute of Molecular Medicine, Radcliffe Department of Medicine, University of Oxford, Oxford, United Kingdom

[10]University of Oxford, Department of Biochemistry, Oxford, United Kingdom

[#] These authors contributed equally to this work.

Abstract

What causes the tissue-specific pathology of diseases resulting from mutations in housekeeping genes? Specifically, in Spinocerebellar ataxia type 7 (SCA7), a neurodegenerative disorder caused by a CAG repeat expansion in *ATXN7*- an essential component of the mammalian transcription co-activation complex, STAGA- the factors underlying the characteristic progressive cerebellar and retinal degeneration observed in patients were unknown. We found that STAGA is required for the transcription initiation of miR-124, which in turn mediates the post-transcriptional crosstalk between lnc-SCA7, a conserved long noncoding RNA, and *ATXN7*. In SCA7, mutations in *ATXN7* disrupt these regulatory interactions and result in a neuron-specific increase in *ATXN7* abundance.

°Corresponding author – anaclaudia.marques@unil.ch.
°Current Address: University of Lausanne, Department of Physiology, Lausanne, Switzerland
§Contributed equally.

AUTHOR CONTRIBUTIONS: ACM conceived the study; JYT performed experiments and analysed results with contributions from KWV, MAV, TS, LMW, HJC, MM, SA, BS, SC, TN and PLO; NB, TF, AB, AS, MJW, CPP and ACM supervised the analysis; CPP and ACM supervised the study; JYT, CPP and ACM wrote the manuscript. All authors read, contributed and agreed with the final version of the manuscript.

Europe PMC Funders Author Manuscripts

Strikingly in mouse, this increase is most prominent in the SCA7 disease-relevant tissues, namely the retina and cerebellum. Our results illustrate how noncoding RNA-mediated feedback regulation of a ubiquitously expressed housekeeping gene may contribute to specific neurodegeneration.

Europe PMC Funders Author Manuscripts

INTRODUCTION

Spinocerebellar ataxia type 7 (SCA7) is a rare inherited neurodegenerative disease that affects approximately 1 in 100,000 births[1]. Like other spinocerebellar ataxias, SCA7 is characterized by uncoordinated movement, abnormal gait, dysarthria, and dysphagia, due to selective neuronal death of Purkinje cells in the cerebellum[2]. Unique to SCA7 is the degeneration of the retinal macula that leads to gradual loss of sight and eventually blindness[3]. SCA7 is caused by an in-frame CAG tri-nucleotide repeat expansion in the first coding exon of the Ataxin type 7 gene, *ATXN7*[2]. Translation of the mutated *ATXN7* allele results in a polyglutamine (polyQ) tract expansion, the formation of protein aggregates and decreased protein activity[4].

ATXN7 is an essential component of the mammalian STAGA multi-protein complex[5] whose chromatin remodelling activity facilitates transcriptional activation of multiple loci. *ATXN7* expression is not specific to the brain, but instead is found at similarly high levels in many non-neuronal tissues, such as the kidney, liver, and lung[2,6]. Why mutations in this ubiquitously expressed housekeeping gene lead to the degeneration of only retinal and cerebellar neurons has remained unresolved.

We hypothesized that regulation by noncoding RNAs, whose expression pattern is often spatially and developmentally restricted[7], might contribute to SCA7's tissue-specific pathology. For instance, aberrant expression of microRNAs (miRNAs) has been previously associated with disease (reviewed in Sayed and Abdellatif, 2011[8]): decreased expression of miR-9 and miR-9* has been found in the cortices of Huntington's disease patients[9], whereas inhibition of miR-19, miR-101, and miR-130 increased the cytotoxicity of polyQ-expanded ATXN1 in Spinocerebellar ataxia type 1[11]. The importance of miRNAs for the survival of neuronal subtypes is clear from the observation that global loss of miRNAs in mouse, achieved by conditional knockout of *Dicer* (*Dcr*, a gene required for miRNA biogenesis), led to the progressive degeneration of specific types of neurons in the CNS, including retinal and cerebellar cells[12,13]. These particular phenotypes are driven, at least in part, by the loss of miR-124, the most abundantly expressed miRNA in the CNS[14] because targeted deletion of this miRNA partially phenocopied *Dcr* knockout and resulted in increased retinal and neuronal cell degeneration[15], the two cell types with the highest miR-124 expression.

Similarly to miRNAs, long (>200 nucleotides) noncoding RNAs (lncRNAs), whose expression is often spatially and temporally restricted[16,17], have also been previously associated with neurodegeneration[18]. Spinocerebellar ataxia type 8 (*SCA8*)[19], for instance, is caused by toxicity of a CUG tri-nucleotide repeat expansion in the lncRNA antisense to *ATNX8* as well as by loss-of-function of the polyQ-expanded mutant ATXN8 protein[20]. As in SCA8, ribonuclear inclusions have been found in other polyQ disorders, such as myotonic dystrophy and Huntington's Disease like type 2[21], suggesting that repeat expanded RNA

may be pathogenic. Long noncoding RNAs can also contribute to disease by regulating the transcript abundance for their overlapping disease-causing gene as found for BACE1-AS, in Alzheimer's disease[22], and for SCAANT1, a noncoding transcript overlapping *ATXN7*[23]. Several intergenic lncRNAs have been found to be dysregulated, compared to controls, in patients with Huntington's[24] or Alzheimer's[25] diseases, and an intergenic lncRNA was recently found to be correlated in expression with a strong intergenic risk allele for Parkinson's disease[26]. However, whether such associations reflect causal contributions by intergenic lncRNAs or else are consequences of the disease pathology remains undetermined.

We sought to establish the origin of the tissue-specific pathology of SCA7 by investigating the regulation of *ATXN7*, a ubiquitously expressed gene, by tissue-specifically expressed noncoding RNAs. Our results demonstrate that the regulation of mutant ATXN7 abundance through crosstalking noncoding RNAs that are highly specific to the retina and the cerebellum contributes to the selective neurodegeneration observed in SCA7.

RESULTS

lnc-SCA7 is a post-transcriptional regulator of *Atxn7*

We identified a retropseudogene, *lnc-SCA7* (also known as *ATXN7L3B*), which is unusually conserved across placental mammals and whose expression is significantly correlated with *ATXN7* across human and mouse adult tissues and postnatal central nervous system (CNS) regions (Figure 1A, Supplementary Figure 1). In mouse, this correlation is stronger in CNS regions (Pearson's R^2=0.94, p<0.001) than elsewhere (Pearson's R^2=0.69, p<0.05, Supplementary Figure 1B), suggesting that an additional layer of regulation could control the relative abundance of both transcripts in these regions.

lnc-SCA7 arose from retrotransposition of *Ataxin-7-like protein 3* (*Atxn7l3*), a distant paralog of *Atxn7*, in the common ancestor of placental mammals approximately 100 million years ago. We found no homology between the 1kb genomic regions upstream of *Atxn7l3* and *lnc-SCA7*, indicating that they are unlikely to have homologous promoters. *lnc-SCA7* inserted downstream of a pre-existing CpG island, and since its duplication accumulated frame-shifting deletions that resulted in premature stop-codons and a truncated open reading frame (ORF) (Supplementary Figure 1C). The small conceptual polypeptide (97 amino acids) encoded by *lnc-SCA7* lacks the two annotated functional ATXN7L3 protein domains (Supplementary Figure 1D). Despite both transcripts being expressed at similarly high levels in mouse neuroblastoma cells (N2A, Supplementary Figure 1E) a custom antibody raised against the N-terminal protein sequence conserved between Atxn7l3 and the putative lnc-SCA7 protein (Supplementary Figure 1C) detected translation of ATXN7L3 (predicted size 39kDa) but not of a polypeptide of the size expected for lnc-SCA7 protein (11kDa, Supplementary Figure 1F, Supplementary Data Set 1). The transcript originating from this gene is thus unlikely to be translated into a stable protein product in these cells.

The coordinated expression between *lnc-SCA7* and *Atxn7* in both mouse and human prompted us to explore whether this long noncoding RNA regulates *Atxn7*'s transcript abundance. In mouse neuroblastoma cells (N2A) cells, lnc-SCA7 depletion (up to 20% of

control) using multiple target-specific short hairpin RNA constructs (*sh-lnc-SCA7*s, Supplementary Figure 2A) significantly reduced *Atxn7* transcript (up to 60% of control, Figure 1B, Supplementary Figure 2B) and protein levels (by approximately 60% of control, Figure 1C, Supplementary Data Set 1). Furthermore, over-expression (6.8-fold) in N2A cells of the region downstream of *lnc-SCA7*'s putative stop-codon (nucleotides 599-3607, hereafter termed *lnc-SCA7-WT*) significantly increased *Atxn7* transcript (2.3-fold, Figure 1D) and protein levels (Figure 1E, Supplementary Data Set 1). Comparable increases in *Atxn7* transcript levels were observed upon over-expression of either full-length lnc-SCA7 sequence or a recombinant mutant with a premature stop codon (Figure 1D, Methods).

We conclude that, in mouse, *lnc-SCA7* modulates the abundance of *Atxn7* via a transcript-dependent mechanism that does not rely on the translation of its putative ORF. Given its cytoplasmic localization (Supplementary Figure 2C), we hypothesized that similarly to other lncRNAs[27] lnc-SCA7 modulates *Atxn7* transcript levels post-transcriptionally by competing for the binding of shared microRNAs (miRNAs).

miR-124 mediates the interaction between lnc-SCA7 and *Atxn7*

To test this hypothesis, we took advantage of a mouse embryonic stem (ES) cell line that is conditionally deficient for Dicer ($Dcr^{\Delta/\Delta}$), an essential component of the miRNA biogenesis pathway in mammals[28]. As observed in N2A cells, we found lnc-SCA7 knockdown (76% relative to control) in wild-type ES cells significantly reduced the expression levels of *Atxn7* (82% of control, Figure 2A). In contrast, in *Dcr*-deficient ES cells a similar level of lnc-SCA7 knock-down had no significant effect on *Atxn7* abundance (Figure 2B). This is consistent with the regulation of *Atxn7* levels by lnc-SCA7 being miRNA-dependent.

Of all brain-expressed miRNAs, only two, miR-16 and miR-124 contain conserved (between mouse and human) predicted miRNA response elements (MREs) within the 3′ UTRs of both *Atxn7* and lnc-SCA7 (Figure 2C, Supplementary Figure 3A-B, Supplementary Table 1). In contrast to miR-16 that has no known role in the brain, miR-124 is the most abundantly expressed miRNA in the CNS[14] and has well established roles in neuronal development[29].

Transfection of N2A cells with miR-124 mimics reduced lnc-SCA7 and *Atxn7* expression levels relative to a non-specific miRNA negative control (32% and 19% of control, respectively; Figure 2D), while reduction of endogenous levels of miR-124 (62% of control) led to significant increase in both lnc-SCA7 and *Atxn7* levels (by 1.8- and 2.5-fold, respectively; Figure 2E). In contrast miR-16 mimics failed to significantly alter the levels of these transcripts (Supplementary Figure 3C). Together with miR-16's considerably lower abundance (Supplementary Figure 3D), these findings indicated that miR-124, but not miR-16, is likely to mediate crosstalk between lnc-SCA7 and *Atxn7* in mouse neurons.

This conclusion was further supported by the reduction in reporter activity upon co-transfection of miR-124 mimics and recombinant lnc-SCA7 or *Atxn7* luciferase reporter constructs (23% and 42% of control, respectively; Figure 2F) being dependent on the presence of the predicted miR-124 MREs in these transcripts. More specifically, inversion of the seed sequences of all miR-124 MREs predicted within lnc-SCA7 (6 MREs) and *Atxn7* (2 MREs) (hereafter referred to as *lnc-SCA7-MUT* and *Atxn7-MUT*, respectively) abolished

the effect of miR-124 on reporter activity (Figure 2F). As expected neither *lnc-SCA7-MUT* nor *Atxn7-MUT* over-expression (7.7 and 9.7-fold, respectively) had a significant impact on *Atxn7* (Figure 2G) or lnc-SCA7 abundance (Figure 2H) consistent with the ability of lnc-SCA7 and *Atxn7* to modulate each other's abundance being miR-124 dependent.

A novel negative feedback loop involving ATXN7 and miR-124

Reduction in lnc-SCA7 levels surprisingly led to depletion of both mature (23% of control, Figure 3A) and precursor miR-124 levels (47% of control, Supplementary Figure 4A). Decreased levels (63% of control) of lnc-SCA7 in human neuroblastoma cells (SH-SY5) was associated with decreased levels of both *ATXN7* (84% of control) and *pri-miR-124a*_1 (87% of control) consistent with the conservation of regulatory interactions in humans (Supplementary Figure 4B). Furthermore and as seen in mouse neuroblastoma cells, decreased levels of endogenous miR-124 are associated with increased lnc-SCA7 and *ATXN7* abundance in these cells (Supplementary Figure 4C), consistent with the evolutionary conservation of crosstalk between these transcripts. Changes in miR-124 levels do not reflect a general effect of lnc-SCA7 on miRNA expression or processing because genome-wide analysis of miRNA abundance revealed no significant differences in N2A miRNA repertoires following either knockdown or over-expression of lnc-SCA7 (Supplementary Table 2, Methods).

This suggested that lnc-SCA7 abundance correlates with the rate of transcription of miR-124 precursor loci and that STAGA might be required for miR-124 transcriptional initiation. To test this hypothesis, we first identified the putative promoters of the three miR-124 precursor genes (*pri-miR-124*s) as their nearest upstream DNAse I hypersensitivity region in the mouse cerebellum that was marked with H3K27ac in that tissue (Supplementary Figure 4D-F). STAGA is required for the transcriptional activation of miR-124 loci: each of these promoters exhibited at least 8.5-fold higher reporter activity than the control antisense sequence (Supplementary Figure 4G) and was bound by Gcn5, STAGA's histone acetyltransferase[5], at 2.0- to 3.5-fold greater levels than IgG control (Figure 3B). Furthermore, while over-expression of *lnc-SCA7-WT* increased luciferase activity for all three miR-124 promoters (1.5- to 1.8-fold), no significant changes in activity were detected following over-expression of *lnc-SCA7-MUT* (Figure 3C). Accordingly, lnc-SCA7 knockdown decreased Gcn5 binding (Supplementary Figure 4H) and luciferase activity for each of the three miR-124 promoters (Supplementary Figure 4I). Furthermore over-expression of *Atxn7-WT* led to a significantly higher increase of miR-124 promoter activity (Supplementary Figure 4J) and mature miR-124 levels (Supplementary Figure 4K) than did *Atxn7*-MUT.

In summary, *Atxn7* promotes miR-124 transcription initiation; in turn this miRNA is key to the post-transcriptional crosstalk between lnc-SCA7, *Atxn7* and other STAGA mRNAs in the CNS (Supplementary Note) predominantly in the tissues in which miR-124 is more highly expressed, namely the retina and the cerebellum (Supplementary Figure 5A-B).

Europe PMC Funders Author Manuscripts

Noncoding RNAs mediate SCA7's tissue specific pathology

In SCA7, the polyQ-expanded ATXN7 protein is associated with decreased STAGA chromatin modification activity[30,31], and with reduced levels of transcripts from loci relying on STAGA transcriptional initiation[32]. The regulatory feedback loop (Figure 4A) revealed by our *in vitro* analysis predicts that a decrease in STAGA activity in SCA7 would result in: (i) diminished *pri-miR-124* transcriptional initiation and, as a consequence, (ii) lowered mature miR-124 and (iii) increased lnc-SCA7 levels (Figure 4B).

We first validated these predictions in a human model of SCA7 by comparing the levels of *ATXN7*, lnc-SCA7 and miR-124 in fibroblasts derived from three SCA7 patients, who carry 42, 49 or 55 polyQ *ATXN7* repeat expansions, against their levels in control fibroblasts (10 polyQ-repeats). Expression levels of miR-124 were reduced by more than two-fold (45% of control), whereas transcript abundances of *lnc-SCA7* and *ATXN7* were increased substantially (by up to 1.8-fold and 5.2-fold, respectively) in these patients' cells (Figure 5A). Furthermore, decreased levels of endogenous miR-124 (62% of control) in human fibroblasts were associated with an increase abundance of both lnc-SCA7 and *ATXN7* (1.22- and 1.27-fold respectively, Supplementary Figure 6), which supports the direct contribution of this miRNA to the post-transcriptional modulation of these two transcripts' levels in fibroblasts.

Furthermore, we predict that changes in miR-124 abundance would result in the post-transcriptional de-repression of mutant *ATXN7* mRNA, and consequently, increased abundance of its encoded protein, with this effect being manifested more prominently in those tissues in which the miRNA most affect *ATXN7* gene abundance. The crosstalk between *ATXN7* and lnc-SCA7 in tissues where miR-124 levels are high is likely to be enhanced which is consistent with their levels' observed higher correlation in the CNS (Supplementary Figure 1B) and might amplify, post-transcriptionally, the impact of changes in miR-124 levels on ATXN7's abundance (Figure 4B). To test the validity of our predictions and the higher impact of noncoding de-regulation in the tissues primarily affected in disease, we took advantage of two established knock-in (KI) SCA7 mouse models, homozygous SCA7$^{100Q/100Q}$ [33] and heterozygous SCA7$^{266Q/5Q}$ [34]. The two models express full-length human *ATXN7* with 100 or 266 CAG (polyQ) repeats inserted into the endogenous mouse *Atxn7* locus. Both mouse models exhibit typical ataxic symptoms, as well as the unique retinal degeneration specific to SCA7[33,34]. Consistent with what is seen in human patients[2], SCA7 mice that carry a higher number of polyQ repeats show earlier disease onset and increased disease severity[34]. We took advantage of the interval separating disease onset for the two SCA7 mouse models and tested our predictions using both symptomatic (aged 28 weeks, SCA7$^{100Q/100Q}$) and pre-symptomatic (aged 5 weeks, SCA7$^{266Q/5Q}$) animals.

First, we investigated whether mutations in *ATXN7* decreases the binding of STAGA upstream of the promoter regions of the three *pri-miR-124*s. Indeed, in the cerebellum of the SCA7$^{100Q/100Q}$ mice, relative to wild-type matched control mice (SCA7$^{5Q/5Q}$), STAGA bound with significantly reduced levels (48-79% reduction) to all 3 *pri-miR-124* promoters (Figure 5B) as expected given our finding that miR-124 loci are targets of the STAGA

complex. Next we compared, between SCA7 KI mice and wild-type controls, the transcript abundances of *ATXN7*, lnc-SCA7 and miR-124 in nine tissues: the two CNS regions primarily affected in disease, namely the retina or cerebellum, four CNS regions largely unaffected by the disease (the striatum, olfactory bulb, cortex and spinal cord), and three non-CNS tissues (muscle, lung and liver). As expected, mature miR-124 levels were significantly decreased in the CNS of SCA7 mouse models where this miRNA is normally more highly expressed (up to 77% of control) resulting in elevated abundance of its targets, lnc-SCA7 (up to 3.8-fold) and *ATXN7* (up to 2.6-fold, Figure 5C, Supplementary Figure 7A-H). As predicted, within the CNS the relative change between wild-type and SCA7 KI in miR-124 levels and associated fold increases in the abundances of lnc-SCA7 and *ATXN7* are highest in the two tissues primarily affected in disease, the retina and the cerebellum (Figure 5C, Supplementary Figure 7A-D). We tested the impact of these changes on the levels of known miR-124 targets[35-44] and found that 8 and 12 out of the 13 transcripts tested were significantly up-regulated in the cerebellum and retina, respectively (Supplementary Figure 7I-J). In contrast, in the three non-CNS tissues tested, muscle, lung and liver, we found no significant change in *ATXN7* or lnc-SCA7 transcript levels in both SCA7 KI mice (Supplementary Figure 7K-O). Absolute *ATXN7* and lnc-SCA7 abundance, measured using droplet digital PCR in the retina, cerebellum, liver and lung of wild-type and SCA7 KI animals is strongly correlated with the levels estimated using standard qRT-PCR (Supplementary Figure 8, Supplementary Table 3). Interestingly, we detected increased levels of mutant *ATXN7* mRNA and reduced levels of miR-124 in the retina and the cerebellum prior to SCA7 onset in the heterozygous SCA7$^{266Q/5Q}$ mice (Figure 5D-E).

Our findings are concordant with crosstalking noncoding RNAs contributing to the tissue-specific disease pathology of SCA7: differences in miR-124, *ATXN7* and lnc-SCA7 levels are more pronounced in the two tissues, retina and cerebellum, that exhibit primary signs of cellular degeneration in SCA7[2].

DISCUSSION

Why mutations in *ATXN7*, a ubiquitously expressed and housekeeping gene, lead to the specific degeneration of retinal and cerebellar neurons observed in SCA7 patients, has thus far remained unexplained. Our in vitro and in vivo analysis in mouse suggests that post-transcriptional regulation by two crosstalking noncoding RNAs, lnc-SCA7 and miR-124, mediates the tissue specificity of SCA7 pathology. Using two SCA7 mouse models, we showed that levels of miR-124 decrease, owing to reduced transcriptional activation activity of the STAGA complex, which in turn is a result of *ATXN7* mutation; thereafter lower miR-124 levels contribute to the increased abundance of *ATXN7* transcripts. These molecular interactions are expected to be more prevalent in the two tissues in which miR-124 is most highly expressed, retina and cerebellum, and in which this miRNA exerts the strongest control on *ATXN7* transcript abundance, which mirrors the cell-specific pathology of SCA7. Post-transcriptional crosstalk between *ATXN7* and lnc-SCA7 is likely to amplify the cellular impact of aberrant miR-124 levels. Nuclear aggregates of mutant ATXN7 protein are often found in the retina and cerebellum of SCA7-affected individuals[34] and although it remains unclear whether these inclusions are the underlying cause or else are a consequence of disease pathology, their presence and the mechanisms leading to their

degradation are associated with increased cytotoxicity and disease severity[45]. In SCA7 patients we propose first that increased levels of mutant ATXN7 protein result from its transcript's cell-specific post-transcriptional de-repression due to lowered miR-124 abundance, and second that these high protein levels lead to increased cytotoxic nuclear inclusions, primarily in the retina and the cerebellum (Figure 4).

miR-124 has been previously associated with neurodegeneration. Its levels are known to be dysregulated in the brain of Huntington's disease patients[9]. Furthermore, some Friedreich's Ataxia (FRDA) patients carry mutations in miR-124 binding sites within the 3′UTR of their *FRDA* (*Frataxin*) gene and these are associated with mRNA up-regulation *in vitro*[46]. Here we have described how cerebellum and retina-specific decreases in miR-124 levels in SCA7 patients contribute to cell-specific degeneration. We show that changes in miR-124 levels also affect the abundance of other known miRNA targets including some that are involved in transcriptional regulation in the cerebellum[47] or in the control of retinal differentiation[48]. We predict that dysregulation of miR-124 targets contributes further to the neuronal specificity of the SCA7 phenotype.

While the contributions of miRNAs to transcriptional regulation and disease are becoming more recognized, those of their longer (>200nt) counterparts remain poorly understood. We have shown that a conserved lncRNA, lnc-SCA7, post-transcriptionally regulates the expression of *ATXN7* as well as many STAGA encoding genes (Supplementary Note). Although the crosstalk between lnc-SCA7 and *ATXN7* is likely to be ubiquitous, as highlighted by their correlated expression levels outside the CNS, it is greatly enhanced in the CNS, most prominently in the retina and the cerebellum, where miR-124 is most abundant. This tissue specificity of the crosstalk between coding and noncoding transcripts supports a functional role for lnc-SCA7 as a key modulator of *ATXN7* abundance in these tissues. Recently, deletion of the 12q21 chromosomal region containing the *lnc-SCA7* and *KCNC2* loci was associated with familiar neurodevelopmental delay and cerebellar ataxia[49]. Both genes were proposed to account for the complex neurodevelopmental phenotype observed in this family[49]. Based on its most prominent crosstalk with *ATXN7* in the cerebellum, we propose that loss-of-function mutations in lnc-SCA7 locus may underlie the ataxia-like symptoms of these individuals.

Our results provide much needed insight into the contributions of noncoding RNAs to human disease, specifically those that confer the cell-specific disease pathology caused by mutations in ubiquitously expressed genes. Identifying additional noncoding RNAs that contribute to the tissue-specificity in other diseases should further improve our understanding of how RNA crosstalk modulates disease phenotypes.

METHODS

Human and mouse gene expression profiling

Microarray gene expression data for *ATXN7* and lnc-SCA7, also known as ATXN7L3B, were obtained from Gene Expression Atlas (GNF) through BioGPS (http://biogps.org) for human[1], and their correlation coefficient (Pearson's correlation, R^2) was computed across all

59 available tissues or cells where both loci were expressed (AD>20, Pearson's R^2 = 0.24, p<0.05, data not shown).

Total RNA from 20 human normal adult tissues (adipose, bladder, brain, cervix, colon, esophagus, heart, kidney, liver, lung, ovary, placenta, prostate, skeletal muscle, small intestine, spleen, testes, thymus, thyroid, and trachea) and 11 mouse normal adult tissues (bladder, brain, colon, heart, kidney, liver, lung, pancreas, skeletal muscle, small intestine, and stomach) were acquired (FirstChoice Human Total RNA Survey Panel, Invitrogen and Amsbio, respectively). Total RNA from 9 mouse (postnatal day 5, pooled from 7 individuals) brain tissues (cerebellum, cortex, entorhinal cortex, hippocampus, hypothalamus, medulla, olfactory bulb, and striatum) was extracted using Trizol (Invitrogen). RNA from mouse retina was extracted from wild-type (WT) C57BL/6 mice (2 pooled individuals) and human retinal RNA was extracted from human WERI neuroblastoma cells using RNeasy kit (Qiagen).

RNA was reverse transcribed into cDNA using QuantiTect Reverse Transcription kit (Qiagen) according to the manufacturer's instructions. Expression levels were estimated by real-time quantitative PCR (qRT-PCR) on a StepOneReal-Time PCR thermocycler (ABI) using SYBR green Master PCR mix (ABI) and loci specific primers (Supplementary Table 4) in triplicate. Non-reverse transcribed RNA was used as negative amplification control.

Western blotting

N2A whole cell extracts were lysed using RIPA buffer (Sigma) and the protein concentration was determined using the BCA assay kit (Pierce). 100μg of protein was loaded onto a 4-20% gradient Tris-Glycine gel (Invitrogen) and separated using gel electrophoresis, transferred onto a PVDF membrane in 1× Transfer buffer (48mM Tris, 39mM Glycine, 20% methanol) at 40V for 2 hrs. Membrane was stained with Ponceau S (Sigma P7170-1L) according to manufacturer guideline and de-stained using water.

Membrane was blocked (5% skimmed milk) for 1 h and incubated overnight in TBST buffer (0.9% NaCl, 100nM Tris, 1% Tween20) with primary antibodies: anti-Atxn7 (sc-21110, Santa Cruz Biotechnology, working dilution 1:200) and custom anti-lnc-SCA7/Atxn7l3 antibody (Amsbio, working dilution 1:100) at 4°C. The membrane was washed 4 times for 30 min in TBST and incubated with biotinylated secondary antibodies [ab6884, ab7089 (Abcam) for Atxn7 and putative lnc-SCA7/Atxn7l3, respectively, 1:5,000] for 1h, followed by washes in TBST, and incubation with horseradish peroxidase-conjugated streptavidin (ab7403, Abcam, 1:10,000) for an additional hour. Enhanced chemiluminescence detection was performed as recommended by the manufacturer (Amersham). The membrane was incubated twice for 10 min in stripping buffer, (25mM Glycine, 1% SDS, and 0.1% Tween 20) followed by two washes in PBS for 10 min and two washes in TBST for 5 min. The membrane was then blocked and re-probed with a positive control antibody, anti-α-tubulin (ab7291, Abcam, working dilution 1:5,000), followed by the procedure described above (secondary antibody, ab64255).

Commercial antibodies were validated by manufacturer as stated in their website. Original images of blots used in this study can be found in Supplementary Data Set 1.

Knockdown and over-expression constructs

Three small interfering RNA (siRNA) constructs, *si-lnc-SCA7s*, were designed using the siRNA selection program from the Whitehead Institute [2] to specifically target lnc-SCA7 (Supplementary Figure 2A, Supplementary Table 4). As a control, we used an oligo with no significant sequence similarity to mRNAs in the mouse genome and with similar nucleotide composition (scrambled control, Supplementary Table 4). siRNAs and scrambled control were used to create short hairpin RNAs (shRNAs) by linking the two arms of the hairpin (loop sequence -TTCAAGAGA). HPLC purified custom-made oligos (10mM, Sigma-Aldrich) were annealed in annealing buffer (10mM Tris pH 8, 50 mM of NaCl) at 95 °C for 5 minutes. After cooling to room temperature, oligos were phosphorylated using T4 Polynucleotide Kinase (NEB) and cloned downstream of a U6 promoter from a modified *pll3.7* vector (courtesy of Dr. Esther Becker). The shRNA construct that had the greatest impact on lnc-SCA7 levels, *sh-lnc-SCA7*, (Supplementary Figure 2B) was used in subsequent experiments. Three stable *lnc-SCA7* knockdown and control N2A polyclonal cell lines were independently derived by co-transfection of the *sh-lnc-SCA7* knockdown and *sh-scrambled* constructs with *pTK-Hyg* (courtesy of Dr. Keith Vance). Cells were grown in hygromycin-containing medium (Invitrogen, 200μg/mL) until high confluence was reached (after approximately 10 days). Medium was changed every 48 hours.

Atxn7 3′ untranslated region (nucleotide 2,876-6,582, ENST00000022257, ENSEMBL Build 70, *Atxn7*-WT) and the putative 3′ noncoding untranslated sequences of mouse *lnc-SCA7* (nucleotide 599 – 3,607, *lnc-SCA7*-WT), the full-length mouse *lnc-SCA7* (*lnc-SCA7*-FULL) as well as *lnc-SCA7*-STOP were cloned downstream of a CMV promoter on the *pcDNA3.1(+)* vector. *lnc-SCA7*-STOP was generated by direct mutagenesis of position 14 of *lnc-SCA7*-FULL from C->A.

To disrupt miR-124 binding sites within *lnc-SCA7*-WT and *Atxn7*-WT, all miR-124 MRE regions complementary to the miRNA seed, 5′-TGCCTT-3′, within these constructs were mutated by reversing the sequence, using direct mutagenesis, to 5′-TTCCGT-3′. Empty *pcDNA3.1(+)* vector was used as transfection control in over-expression experiments.

Tissue culture

Mouse neuroblastoma (N2A) cells were grown, at 37°C in a humidified atmosphere supplemented with 5% CO_2, in *Dulbecco's Modified Eagle Medium* (DMEM) containing antibiotic penicillin/streptomycin, supplemented with 10% Fetal Calf Serum (FCS). Mouse DTCM23/49 XY embryonic stem (ES) cell lines were grown as described previously[3]. Deletion of *Dcr*'s RNAse III domain was induced by culturing the cells in the presence of 800nM (Z)-4-Hydroxytamoxifen (4-OHT, Sigma); non-induced cells were treated with 0.1% ethanol and used as control. Both conditional and *Dcr*-deficient ES cells were routinely maintained on a feeder layer of mitomycin-inactivated mouse primary embryonic fibroblasts. Prior to the analyses, feeder cells were depleted from the cultures by pre-plating trypsinized cells for 25 minutes and transferring ES-enriched cell suspension to a new gelatine-coated plate in a culturing medium supplemented with Leukemia Inhibitory Factor (Invitrogen) and 2i inhibitors (CHIR99021 at 3nM and PD0325901 at 1nM, Stemgent). After removal of the RNase III domain of *Dcr*, cells were kept for no longer than 6 passages.

SCA7 patient-derived fibroblast cell lines ($SCA7^{42Q/10Q}$, $SCA7^{49Q/10Q}$, $SCA7^{55Q/10Q}$) were incubated at 37 °C in 5% CO_2 in DMEM Glutamax (Gibco-BRL) supplemented with 10% FBS and antibiotics.

One day prior to transfection, N2A or ES cells (1.0×10^5 cells/ml) were seeded in 6-well dishes. Knockdown, over-expression and their respective control constructs (1μg) were transfected using FuGENE 6 Transfection Agent (Roche) according to the manufacturer's guideline. After transfection, cells were grown under standard conditions prior to harvesting. A miRNA's mimic (50nM/well) (mirVana, ABI), and its negative control (Cat. No. 4464058, ABI), or a siRNA (5nM/well) (FlexiTube GS382423, Qiagen), and its negative control (Cat. No. 1027280, Qiagen), were transfected using Lipofectamine RNAiMAX Reagent (Invitrogen). Cells were harvested 48h post-transfection.

RNA extraction and quantification

Total cellular RNA was extracted using the RNeasy kit (Qiagen) following the manufacturer's instructions. To quantify levels of mature miRNAs, total RNA was extracted using the miRNeasy kit (Qiagen). Genomic DNA was removed using the DNA-free kit (Ambion). RNA was reversed transcribed and cDNA used to quantify gene expression changes, relative to *Gadph*, using sequence specific primers (Supplementary Table 4), as described above.

For miRNA quantification RNA was reverse transcribed using TaqMan MicroRNA Reverse Transcription Kit (Invitrogen). For comparison of miRNA expression between tissues, RNA was reverse transcribed using the NCode VILO miRNA cDNA Synthesis Kit (Invitrogen). miRNA abundance was measured by qRT-PCR (SYBR green) using miRNA-specific TaqMan MicroRNA Assays (ABI) according to the manufacturer's instructions. The expression levels of miRNAs were normalized to that of 18S rRNA.

Mutagenesis

Directed mutagenesis of constructs were generated by PCR using 2μl of reverse transcribed cDNA with 300mM of primers (Supplementary Table 4), 1U Expand High Fidelity DNA polymerase (Roche), 1.5mM MgCl2, 0.2mM dNTPs, 5% DMSO and 10x buffer in 50μl total volume. PCR reaction was carried out in a Veriti 96-well (Applied Biosystems) thermocycler as following: 94°C for 2min, followed by 5 cycles with 15s at 94°C, 15s at a temperature gradient of 58 – 68°C and 2min at 94°C, followed by 15 cycles with 15s at 94°C, 30s at a temperature gradient of 55 – 65°C and 2min at 72°C with 5s extension added after each cycle, followed by a terminal step at 72°C for 7min. All constructs were verified by sanger sequencing.

Subcellular fractionation

Subcellular fractionation of N2A cells was carried out using the PARIS kit (Invitrogen) following manufacturer's instructions. After isolating the nuclear and cytoplasmic fractions from total cell lysates, RNA from each subcellular compartment was extracted, reverse transcribed, and quantified as described above. Using qRT-PCR, expression levels of all genes were measured independently in the cytoplasmic and nuclear fractions. Fold

enrichment between the distinct compartments (expression level measured in the cytoplasmic/expression level measured in the nucleus) was reported after normalization to *Gapdh*.

Luciferase assays

lnc-SCA7 and *Atxn7* 3′ UTRs were cloned downstream of the luciferase reporter gene in the *pGL3-promoter* (*pGL3-pro*) vector (Promega), *luc-lnc-SCA7*-WT and *luc-Atxn7*-WT, respectively. *luc-lnc-SCA7*-MUT and *luc-Atxn7*-MUT were generated by directed mutagenesis of all miR-124 binding sites. Each luciferase construct (2μg) was co-transfected with 10ng of pRL-*Renilla* luciferase control vector (Promega) and 50nM mirVana miR-124 or negative miRNA control mimics (miR-NC) (Invitrogen) using the FuGENE 6 Transfection Agent (Roche).

Putative promoter elements of the three *pri-miR-124s* (*miR-124_1*: chr14:65,205,705 – 65,207,200; *miR-124_2*: chr3:17,694,143 – 17,695,600; *miR-124_3*: chr2:180,627,439 – 180,628,900, mm9) and Negative control (NC chr14:65,183,839 – 65,185,271, mm9) were cloned upstream of the luciferase reporter gene in the *pGL3-enhancer* (*pGL3-enh*) vector (Promega): miR-124-1-prom-luc, miR-124-2-prom-luc miR-124-3-prom-luc and *NC-prom-luc*. As control, the same sequences were cloned into the same location in the reverse orientation. Constructs were transfect at the same concentration and using the same conditions as described above Following transfection, N2A cells were grown under standard conditions for 48h before harvesting. Dual luciferase activity was measured using the Dual-luciferase reporter assay system (Promega) according to the manufacturer's guideline on the FLUOstar OPTIMA (BMG Labtech) fluorescence plate reader. Luciferase activity was normalized against measured *Renilla* activity (transfection control) as proposed by the manufacturer.

Prediction of miRNA response elements

miRNA response elements (MREs) for the human lnc-SCA7 (*ATXN7L3B*), *ATXN7* and STAGA-subunit encoding mRNAs (obtained from neXtProt.com[4]) were downloaded from microRNA.org (all mirSVR scores)[5]. The observed percentage of shared MREs between lnc-SCA7 and STAGA encoding subunits was compared to the fraction of shared MREs found across 10,000 randomly selected sets of brain-expressed 23 genes that are not part of the STAGA complex (all mirSVR scores, microRNA.org). An empirical *p*-value was calculated by comparing the number of MREs shared between lnc-SCA7 and the STAGA mRNAs with those shared between lnc-SCA7 and the randomized sets of brain-expressed 23 genes. MREs predicted to be shared between lnc-SCA7 and STAGA encoding mRNAs or randomly selected mRNAs were represented using Circos plots [6] (circos.ca).

Genome-wide analysis of miRNA abundance

N2A cells were transfected with *sh-lnc-SCA7* or scramble control (1μg) and *lnc-SCA7*-WT, *lnc-SCA7*-MUT over-expression constructs or *pcDNA3.1(+)* empty vector control (1μg). Cells were harvested and total RNA was extracted using the miRNeasy kit (Qiagen) 48 hours post-transfection. Four biological replicates were performed for each experimental condition. A total of 611 mouse and murine virus-associated miRNAs were quantified using

the nCounter miRNA Expression Assay (NanoString Technologies, Seattle, WA)[7] according to the manufacturer's instructions. Briefly, input RNA (105ng) and miRtag linkers were ligated prior to hybridization with barcoded reporter and biotinylated capture probes at 65°C for 16h. Samples were prepared for analysis on the nCounter Prep Station before data was collected at 555 FOV on the nCounter Digital Analyzer.

Data were analysed using NanoString Differential Expression (NanoStriDE[8]) interface. After normalization using a set of house-keeping mRNAs and multiple test correction using *t-test*, the genome-wide analysis of miRNA abundance revealed no significant differences in N2A's miRNA repertoires following either knockdown or over-expression of *lnc-SCA7* (Supplementary Table 4). Although changes in miR-124 levels were not genome-wide significant, the trends observed by qRT-PCR could be replicated in this experiment. We attribute the lack of genome significance to reduced power to detect transcripts expressed at miR-124 levels using the standard protocol. We do not detect differences for highly abundant miRNAs, consistent with no global changes in miRNA repertoires.

Chromatin Immunoprecipitation (ChIP)

Wild-type N2As and three independently derived polyclonal N2A cell lines stably expressing *sh-lnc-SCA7* or control shRNA (*sh-scramble*) were directly cross-linked for 10 min at 37°C by adding 1% formaldehyde to the tissue culture medium. For mouse cerebellar tissue, dissected samples were dounced in PBS using a homogenizer to generate a single cell suspension. 1% final concentration formaldehyde was added and the samples were incubated for 10 min at room temperature with rotation. Cross-linking reactions were quenched using 0.125M glycine. Nuclei were isolated and chromatin sheared to approximately 500bp using a Bioruptor (Diagenode). 1mg cross-links was immunoprecipitated using 5ug anti-rabbit GCN5 (Santa Cruz H-75) or anti-rabbit IgG control (Millipore) antibodies overnight at 4°C. Complexes were collected using Protein-A magnetic beads (Pierce), washed, eluted and the cross-links were reversed at 65°C overnight. DNA was precipitated, treated with Proteinase K (Roche) and purified using a PCR Purification Kit (Qiagen).

We tested STAGA-binding across five consecutive regions (250bp in length) upstream of each transcriptional start site (TSS) of miR-124 precursor transcripts (*pri-miR-124*) annotated by the ENCODE consortium (UCSC browser)[9] as sensitive to DNAse I treatment and enriched in H3K27ac marks in the cerebellum within: chr14:65,205,705 – 65,207,200, chr3:17,694,143 – 17,695,600, and chr2:180,627,439 – 180,628,900 for *pre-miR-124-1, -2* and *-3*, respectively (Supplementary Figure 4D-F). The control region (chr14:65,183,839 – 65,185,271) was selected based on its lack of DNAse I and H3K27ac marks and its proximity to the predicted STAGA bound regions (Supplementary Figure 4D). Primers used to detect all regions were designed with a similar nucleotide composition (Supplementary Table 4). Specific enrichment of Gcn5 relative to IgG was determined from three independent ChIP assays by qPCR.

SCA7 knock-in mouse models

SCA7$^{100Q/5Q}$ knock-in mice carrying 100 CAG repeats on the pathological allele in the mouse Sca7 locus were kindly provided by Dr. H. Y. Zoghbi [10]. Heterozygous SCA7$^{100Q/5Q}$ males were mated with SCA7$^{100Q/5Q}$ females. Genotyping was as described previously[11]. Homogenous SCA7$^{100Q/100Q}$ male animals (aged 28 weeks, *n* = 4) were used for subsequent RNA quantification by qRT-PCR and by *in-situ* hybridization. The experiments were carried out in accordance with the Guide for the Care and Use of Laboratory Animals (National Research Council 1996), European Directive N°86/609 and the guidelines of the local institutional animal care and use committee. The study was approved (06/26/2010) by the local Institutional Review Board (Direction Générale pour la Recherche et l'Innovation). SCA7$^{266Q/5Q}$ mice[11] were obtained from the Jackson Laboratories (stock number 008682) and maintained by crossing heterozygous SCA7$^{266Q/5Q}$ with wild-type 5Q/5Q animals. Genotyping was performed as previously described[11]. Heterozygous SCA7$^{266Q/5Q}$ male animals (aged 5 weeks, *n* = 3) were used for subsequent RNA quantification by qRT-PCR and *in-situ* hybridization. Experiments were carried out according to United Kingdom Home Office Animals (Scientific Procedures) Act 1986 and local ethical approval from the University of Oxford. In both cases, the mice were maintained on a 12h light/dark cycle with access *ad libitum* to food and water. Only regions with the highest Gcn5 binding found in N2As was tested in the cerebellum of SCA7$^{100Q/100Q}$: namely 1a, 2b, 3c, na for miR-124-1, miR-124-2, miR-124-3 and negative control region, respectively.

Tissue preparation for RNA analyses

Tissues of homozygous SCA7$^{100Q/100Q}$ mice at the late stage of disease (28 weeks of age, *n* = 4) and wild-type age- and sex-matched controls (n = 2) were used to perform qRT-PCR expression analyses. *In situ* hybridization and qRT-PCR was also carried out from heterozygous SCA7$^{266Q/5Q}$ mice (5 weeks of age, *n* = 3 for both experiments) and wild-type age- and sex- matched littermate controls (SCA7$^{5Q/5Q}$, *n* = 3 for each experiment). Biopsies from neuronal tissues (retina, cerebellum, cortex, striatum, olfactory bulb, and spinal cord) were collected at 4°C using an adult mouse brain matrix slicer. Non-neuronal tissues (liver, lung and muscle) were dissected at 4°C. After dissection, biopsies were immediately frozen in liquid nitrogen and stored at −80°C until RNA extraction. Tissues were homogenized in RLT buffer with 1% β-mercaptoethanol (RNeasy kit, Qiagen) and prepared for RNA extraction as described previously. Reverse transcription to cDNA was performed as described previously followed by gene expression detection by qRT-PCR.

In-situ hybridization

Target sequences were generated by PCR or qRT-PCR, cloned into pCR4-TOPO (Invitrogen) and digoxigenin (DIG)-labelled riboprobes were synthesised from linearized plasmid DNA. Tissue samples were snap frozen in OCT (VWR) and 14μm sections were cut using a cryostat (Leica) and mounted onto Superfrost Plus slides (VWR). For *Atxn7*, probe hybridization, washing and signal detection using an alkaline-phosphatase conjugated anti-DIG antibody was carried out as previously described [12]. Sense strand probes were also tested to obtain a negative control signal (data not shown). Primer sequences for riboprobe cloning of *lnc-SCA7* and *Atxn7* can be found in Supplementary Table 4. For miR-124, a

DIG-labelled LNA probe (Exiqon) was hybridized as above with some slight modifications [13]. To ensure signals obtained prior to analysis were at sub-saturation levels, the *Atxn7* probe was hybridized for 16 hours, whereas the miR-124 probe was hybridized for 4 hours.

SCA7 patient fibroblasts

Transcript abundance of SCA7 fibroblast cell lines against that of a control fibroblast cell line (10Q/10Q) was quantified by qRT-PCR using SYBR green Master PCR mix (Invitrogen) and target-specific primers in combination with a TaqMan (Invitrogen) probe (*ATXN7*: Cat. No. 4331182, Invitrogen; *GAPDH*: Cat. No. 4331182, Invitrogen; custom made lnc-SCA7 probe (Supplementary Table 4)). Results illustrated in Figure 5A were measured using sensitive TaqMan-based qRT-PCR. Ethics approval for the establishment of patient fibroblast cultures was granted by the University of Cape Town (UCT) Faculty of Health Sciences Human Research Ethics Committee (HREC REF. 380/2009 and 434/2011), and was renewed annually.

Statistics

All expression correlation comparisons were determined using the Pearson's correlation test and all differential expression comparisons were determined using Student's *t*-test. Asterisks indicate significance in the level of the comparison between the expression of target transcripts (* $p<0.05$; ** $p<0.01$; *** $p<0.001$; NS [not significant] $p>0.05$). For each experimental analysis statistical values are calculated using data collected from three independent experiments.

SUPPLEMENTARY MATERIAL

Refer to Web version on PubMed Central for supplementary material.

Acknowledgments

We thank Esther Becker for vectors, helpful discussions and comments on the manuscript; Alun Barnard, Michelle McClements, and Robert MacLaren for WERI cells; and members of the ACM and CPP groups for insightful comments and suggestions; Ingrid Baumgarten for valuable discussions and establishing patient fibroblast cultures; Huda Y Zoghbi for the SCA7$^{100Q/5Q}$ mice. This work was funded by the Medical Research Council (CPP; WIMM Strategic Award, MRC #G0902418 BS, TAF), a Marie Curie Intra-European Career Development Award (ACM), the University of Oxford (ACM), the Royal Society (ACM), a European Research Council Advanced Grant (CPP, ACM, KVW, TS), the National Research Foundation SA (LMW), Medical Research Council SA (LMW), University of Cape Town (LMW), Harry Crossley Foundation (LMW), Commonwealth Scholarship Commission (LMW), Clarendon Fund (JYT), the Natural Sciences Engineering Research Council of Canada (JYT), the Wellcome Trust (WT081385 SC, TN, NB), a European Research Council Starting Grant (PLO), Ataxia UK (HJC, MAV), French Association against Myopathies (AFM, to AB and long-term fellowship to SA), the French Association *Connaitre les Syndrômes Cérébelleux* (AS, SA) and the French Ministry of Research (fellowship to MM).

REFERENCES

1. Gouw LG, et al. Analysis of the dynamic mutation in the SCA7 gene shows marked parental effects on CAG repeat transmission. Human molecular genetics. 1998; 7:525–532. doi: 10.1093/Hmg/7.3.525. [PubMed: 9467013]
2. David G, et al. Cloning of the SCA7 gene reveals a highly unstable CAG repeat expansion. Nat Genet. 1997; 17:65–70. doi: 10.1038/Ng0997-65. [PubMed: 9288099]

3. Aleman TS, et al. Retinal degeneration associated with spinocerebellar ataxia type 7 (SCA7). Invest Ophthalmol Vis Sci. 2000; 41:S175–S175.
4. Holmberg M, et al. Spinocerebellar ataxia type 7 (SCA7): a neurodegenerative disorder with neuronal intranuclear inclusions. Human molecular genetics. 1998; 7:913–918. doi: 10.1093/Hmg/7.5.913. [PubMed: 9536097]
5. Helmlinger D, et al. Ataxin-7 is a subunit of GCN5 histone acetyltransferase-containing complexes. Human molecular genetics. 2004; 13:1257–1265. doi: 10.1093/Hmg/Ddh139. [PubMed: 15115762]
6. Cancel G, et al. Distribution of ataxin-7 in normal human brain and retina. Brain. 2000; 123(Pt 12): 2519–2530. [PubMed: 11099453]
7. Mattick JS. The genetic signatures of noncoding RNAs. Plos Genet. 2009; 5:e1000459. doi: 10.1371/journal.pgen.1000459. [PubMed: 19390609]
8. Sayed D, Abdellatif M. MicroRNAs in development and disease. Physiol Rev. 2011; 91:827–887. doi: 10.1152/physrev.00006.2010. [PubMed: 21742789]
9. Packer AN, Xing Y, Harper SQ, Jones L, Davidson BL. The bifunctional microRNA miR-9/miR-9* regulates REST and CoREST and is downregulated in Huntington's disease. J Neurosci. 2008; 28:14341–14346. doi: 10.1523/JNEUROSCI.2390-08.2008. [PubMed: 19118166]
10. Johnson R, Buckley NJ. Gene dysregulation in Huntington's disease: REST, microRNAs and beyond. Neuromolecular medicine. 2009; 11:183–199. doi: 10.1007/s12017-009-8063-4. [PubMed: 19458943]
11. Lee Y, et al. miR-19, miR-101 and miR-130 co-regulate ATXN1 levels to potentially modulate SCA1 pathogenesis. Nat Neurosci. 2008; 11:1137–1139. doi: 10.1038/nn.2183. [PubMed: 18758459]
12. Damiani D, et al. Dicer inactivation leads to progressive functional and structural degeneration of the mouse retina. The Journal of neuroscience. 2008; 28:4878–4887. doi: 10.1523/JNEUROSCI.0828-08.2008. [PubMed: 18463241]
13. Schaefer A, et al. Cerebellar neuro degeneration in the absence of microRNAs. J Exp Med. 2007; 204:1553–1558. doi: 10.1084/Jem.20070823. [PubMed: 17606634]
14. Lagos-Quintana M, et al. Identification of tissue-specific microRNAs from mouse. Curr Biol. 2002; 12:735–739. doi: 10.1016/S0960-9822(02)00809-6. [PubMed: 12007417]
15. Sanuki R, et al. miR-124a is required for hippocampal axogenesis and retinal cone survival through Lhx2 suppression. Nat Neurosci. 2011; 14:1125–U1177. doi: 10.1038/Nn.2897. [PubMed: 21857657]
16. Derrien T, et al. The GENCODE v7 catalog of human long noncoding RNAs: analysis of their gene structure, evolution, and expression. Genome Res. 2012; 22:1775–1789. doi: 10.1101/gr.132159.111. [PubMed: 22955988]
17. Cabili MN, et al. Integrative annotation of human large intergenic noncoding RNAs reveals global properties and specific subclasses. Genes and development. 2011; 25:1915–1927. doi: 10.1101/gad.17446611. [PubMed: 21890647]
18. Qureshi IA, Mattick JS, Mehler MF. Long non-coding RNAs in nervous system function and disease. Brain Res. 2010; 1338:20–35. doi: 10.1016/j.brainres.2010.03.110. [PubMed: 20380817]
19. Koob MD, et al. An untranslated CTG expansion causes a novel form of spinocerebellar ataxia (SCA8). Nat Genet. 1999; 21:379–384. doi: 10.1038/7710. [PubMed: 10192387]
20. Daughters RS, et al. RNA Gain-of-Function in Spinocerebellar Ataxia Type 8. Plos Genet. 2009; 5 doi: 10.1371/journal.pgen.1000600.
21. La Spada AR, Taylor JP. Repeat expansion disease: progress and puzzles in disease pathogenesis. Nat Rev Genet. 2010; 11:247–258. doi: 10.1038/nrg2748. [PubMed: 20177426]
22. Faghihi MA, et al. Evidence for natural antisense transcript-mediated inhibition of microRNA function. Genome Biol. 2010; 11 doi: 10.1186/Gb-2010-11-5-R56.
23. Sopher BL, et al. CTCF Regulates Ataxin-7 Expression through Promotion of a Convergently Transcribed, Antisense Noncoding RNA. Neuron. 2011; 70:1071–1084. doi: 10.1016/j.neuron.2011.05.027. [PubMed: 21689595]
24. Bithell A, Johnson R, Buckley NJ. Transcriptional dysregulation of coding and non-coding genes in cellular models of Huntington's disease. Biochem Soc Trans. 2009; 37:1270–1275. doi: 10.1042/BST0371270. [PubMed: 19909260]

25. Mus E, Hof PR, Tiedge H. Dendritic BC200 RNA in aging and in Alzheimer's disease. Proc Natl Acad Sci U S A. 2007; 104:10679–10684. doi: 10.1073/pnas.0701532104. [PubMed: 17553964]
26. Kumar V, et al. Human disease-associated genetic variation impacts large intergenic non-coding RNA expression. Plos Genet. 2013; 9:e1003201. doi: 10.1371/journal.pgen.1003201. [PubMed: 23341781]
27. Tay Y, Rinn J, Pandolfi PP. The multilayered complexity of ceRNA crosstalk and competition. Nature. 2014; 505:344–352. doi: 10.1038/nature12986. [PubMed: 24429633]
28. Nesterova TB, et al. Dicer regulates Xist promoter methylation in ES cells indirectly through transcriptional control of Dnmt3a. Epigenetics Chromatin. 2008; 1 doi: 10.1186/1756-8935-1-2.
29. Visvanathan J, Lee S, Lee B, Lee JW, Lee SK. The microRNA miR-124 antagonizes the anti-neural REST/SCP1 pathway during embryonic CNS development. Genes Dev. 2007; 21:744–749. doi: 10.1101/gad.1519107. [PubMed: 17403776]
30. McMahon SJ, Pray-Grant MG, Schieltz D, Yates JR, Grant PA. Polyglutamine-expanded spinocerebellar ataxia-7 protein disrupts normal SAGA and SLIK histone acetyltransferase activity. Proc Natl Acad Sci U S A. 2005; 102:8478–8482. doi: 10.1073/pnas.0503493102. [PubMed: 15932941]
31. Palhan VB, et al. Polyglutamine-expanded ataxin-7 inhibits STAGA histone acetyltransferase activity to produce retinal degeneration. Proc Natl Acad Sci U S A. 2005; 102:8472–8477. doi: 10.1073/pnas.0503505102. [PubMed: 15932940]
32. McCullough SD, et al. Reelin is a target of polyglutamine expanded ataxin-7 in human spinocerebellar ataxia type 7 (SCA7) astrocytes. Proceedings of the National Academy of Sciences of the United States of America. 2012; 109:21319–21324. doi: 10.1073/pnas.1218331110. [PubMed: 23236151]
33. Chen YC, et al. Gcn5 loss-of-function accelerates cerebellar and retinal degeneration in a SCA7 mouse model. Human molecular genetics. 2012; 21:394–405. doi: 10.1093/hmg/ddr474. [PubMed: 22002997]
34. Yoo SY, et al. SCA7 knockin mice model human SCA7 and reveal gradual accumulation of mutant ataxin-7 in neurons and abnormalities in short-term plasticity. Neuron. 2003; 37:383–401. [PubMed: 12575948]
35. Karginov FV, et al. A biochemical approach to identifying microRNA targets. Proc Natl Acad Sci U S A. 2007; 104:19291–19296. doi: 10.1073/pnas.0709971104. [PubMed: 18042700]
36. Agirre X, et al. Epigenetic silencing of the tumor suppressor microRNA Hsa-miR-124a regulates CDK6 expression and confers a poor prognosis in acute lymphoblastic leukemia. Cancer research. 2009; 69:4443–4453. doi: 10.1158/0008-5472.CAN-08-4025. [PubMed: 19435910]
37. Yoo AS, Staahl BT, Chen L, Crabtree GR. MicroRNA-mediated switching of chromatin-remodelling complexes in neural development. Nature. 2009; 460:642–646. doi: 10.1038/nature08139. [PubMed: 19561591]
38. Makeyev EV, Zhang J, Carrasco MA, Maniatis T. The MicroRNA miR-124 promotes neuronal differentiation by triggering brain-specific alternative pre-mRNA splicing. Mol Cell. 2007; 27:435–448. doi: 10.1016/j.molcel.2007.07.015. [PubMed: 17679093]
39. Liu XS, et al. MicroRNA Profiling in Subventricular Zone after Stroke: MiR-124a Regulates Proliferation of Neural Progenitor Cells through Notch Signaling Pathway. PloS one. 2011; 6 doi: 10.1371/journal.pone.0023461.
40. Shi XB, et al. Tumor suppressive miR-124 targets androgen receptor and inhibits proliferation of prostate cancer cells. Oncogene. 2013; 32:4130–4138. doi: 10.1038/Onc.2012.425. [PubMed: 23069658]
41. Xia H, et al. Loss of brain-enriched miR-124 microRNA enhances stem-like traits and invasiveness of glioma cells. J Biol Chem. 2012; 287:9962–9971. doi: 10.1074/jbc.M111.332627. [PubMed: 22253443]
42. Hendrickson DG, Hogan DJ, Herschlag D, Ferrell JE, Brown PO. Systematic identification of mRNAs recruited to argonaute 2 by specific microRNAs and corresponding changes in transcript abundance. PloS one. 2008; 3:e2126. doi: 10.1371/journal.pone.0002126. [PubMed: 18461144]

43. Fang M, et al. The miR-124 regulates the expression of BACE1/beta-secretase correlated with cell death in Alzheimer's disease. Toxicology letters. 2012; 209:94–105. doi: 10.1016/j.toxlet.2011.11.032. [PubMed: 22178568]
44. Nakamachi Y, et al. MicroRNA-124a is a key regulator of proliferation and monocyte chemoattractant protein 1 secretion in fibroblast-like synoviocytes from patients with rheumatoid arthritis. Arthritis and rheumatism. 2009; 60:1294–1304. doi: 10.1002/art.24475. [PubMed: 19404929]
45. Zander C, et al. Similarities between spinocerebellar ataxia type 7 (SCA7) cell models and human brain: proteins recruited in inclusions and activation of caspase-3. Human molecular genetics. 2001; 10:2569–2579. doi: 10.1093/hmg/10.22.2569. [PubMed: 11709544]
46. Bandiera S, et al. Genetic variations creating microRNA target sites in the FXN 3′-UTR affect frataxin expression in Friedreich ataxia. PloS one. 2013; 8:e54791. doi: 10.1371/journal.pone.0054791. [PubMed: 23382970]
47. Chou AH, et al. Polyglutamine-expanded ataxin-7 causes cerebellar dysfunction by inducing transcriptional dysregulation. Neurochem Int. 2010; 56:329–339. doi: 10.1016/j.neuint.2009.11.003. [PubMed: 19909779]
48. Abou-Sleymane G, et al. Polyglutamine expansion causes neurodegeneration by altering the neuronal differentiation program. Human molecular genetics. 2006; 15:691–703. doi: 10.1093/Hmg/Ddi483. [PubMed: 16434483]
49. Brandenberger R, et al. Identification and characterization of a novel extracellular matrix protein nephronectin that is associated with integrin alpha8beta1 in the embryonic kidney. J Cell Biol. 2001; 154:447–458. [PubMed: 11470831]

METHODS REFERENCES

1. Su AI, et al. A gene atlas of the mouse and human protein-encoding transcriptomes. Proc Natl Acad Sci U S A. 2004; 101:6062–6067. doi: 10.1073/pnas.0400782101. [PubMed: 15075390]
2. Yuan B, Latek R, Hossbach M, Tuschl T, Lewitter F. siRNA Selection Server: an automated siRNA oligonucleotide prediction server. Nucleic acids research. 2004; 32:W130–134. doi: 10.1093/nar/gkh366. [PubMed: 15215365]
3. Nesterova TB, et al. Dicer regulates Xist promoter methylation in ES cells indirectly through transcriptional control of Dnmt3a. Epigenetics Chromatin. 2008; 1 doi: 10.1186/1756-8935-1-2.
4. Lane L, et al. neXtProt: a knowledge platform for human proteins. Nucleic acids research. 2012; 40:D76–83. doi: 10.1093/nar/gkr1179. [PubMed: 22139911]
5. Betel D, Wilson M, Gabow A, Marks DS, Sander C. The microRNA.org resource: targets and expression. Nucleic acids research. 2008; 36:D149–153. microRNA.org. doi: 10.1093/nar/gkm995. [PubMed: 18158296]
6. Krzywinski M, et al. Circos: an information aesthetic for comparative genomics. Genome Res. 2009; 19:1639–1645. doi: 10.1101/gr.092759.109. [PubMed: 19541911]
7. Geiss GK, et al. Direct multiplexed measurement of gene expression with color-coded probe pairs. Nature biotechnology. 2008; 26:317–325. doi: 10.1038/nbt1385.
8. Brumbaugh CD, Kim HJ, Giovacchini M, Pourmand N. NanoStriDE: normalization and differential expression analysis of NanoString nCounter data. BMC bioinformatics. 2011; 12:479. doi: 10.1186/1471-2105-12-479. [PubMed: 22177214]
9. ENCODE Project Consortium. Myers RM, et al. A User's Guide to the Encyclopedia of DNA Elements (ENCODE). Plos Biol. 2011; 9:e1001046. doi: 10.1371/journal.pbio.1001046. [PubMed: 21526222]
10. Chen YC, et al. Gcn5 loss-of-function accelerates cerebellar and retinal degeneration in a SCA7 mouse model. Human molecular genetics. 2012; 21:394–405. doi: 10.1093/hmg/ddr474. [PubMed: 22002997]
11. Yoo SY, et al. SCA7 knockin mice model human SCA7 and reveal gradual accumulation of mutant ataxin-7 in neurons and abnormalities in short-term plasticity. Neuron. 2003; 37:383–401. [PubMed: 12575948]

12. Chodroff RA, et al. Long noncoding RNA genes: conservation of sequence and brain expression among diverse amniotes. Genome Biol. 2010; 11:R72. doi: 10.1186/gb-2010-11-7-r72. [PubMed: 20624288]

13. Deo M, Yu JY, Chung KH, Tippens M, Turner DL. Detection of mammalian microRNA expression by in situ hybridization with RNA oligonucleotides. Developmental dynamics. 2006; 235:2538–2548. doi: 10.1002/dvdy.20847. [PubMed: 16736490]

Europe PMC Funders Author Manuscripts

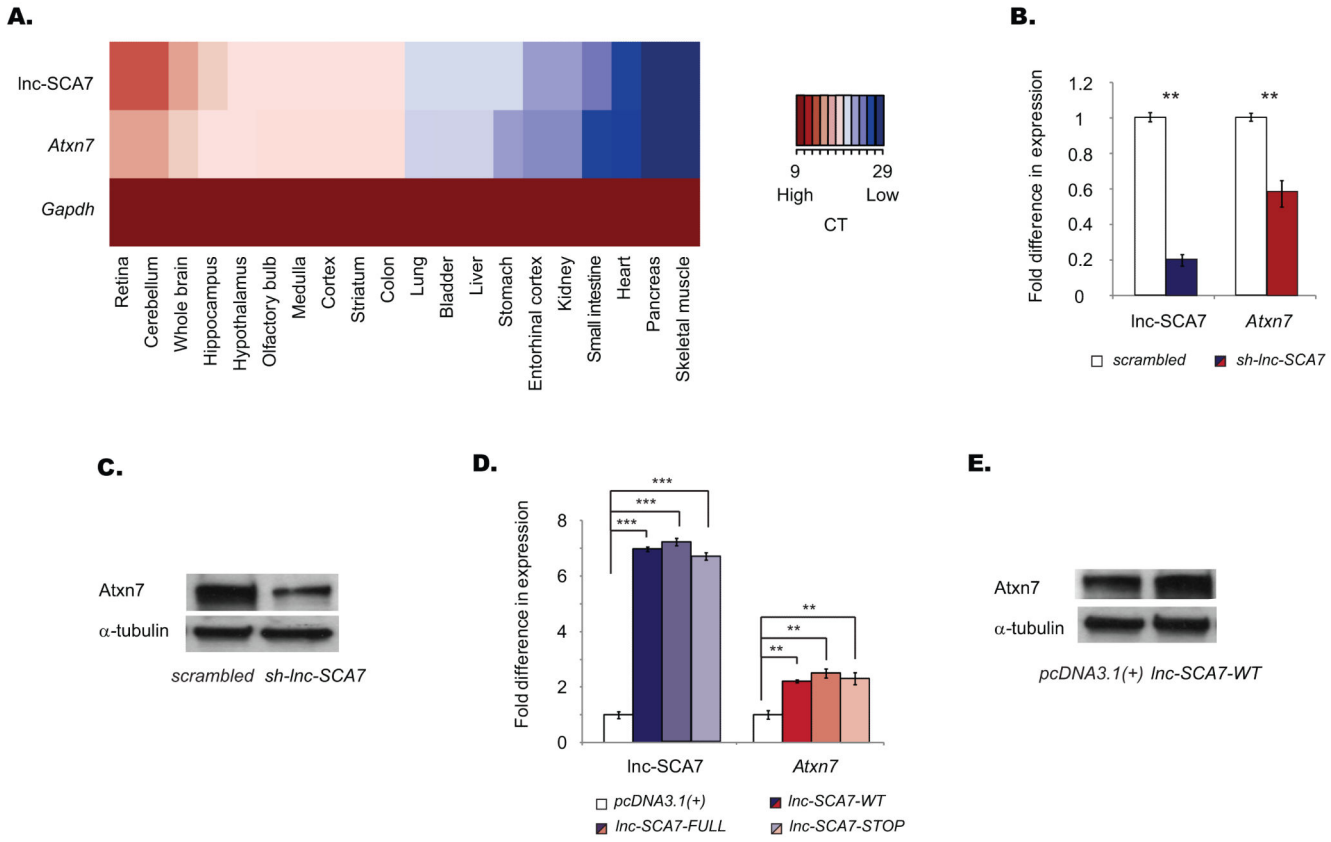

Figure 1. *lnc-SCA7* regulates *Atxn7* abundance

(A) Heatmap representing expression levels measured by qRT-PCR using sequence specific primers (Supplementary Table 4) [cross-threshold cycle (CT)] of lnc-SCA7, *Atxn7* and *Gapdh* (control) (*n = 3* biological replicates per tissue sample). (B) Fold difference in expression (y-axis) in N2A cells upon knockdown of lnc-SCA7 (blue) was associated with a significant reduction in *Atxn7* (red) transcript abundance (C) and reduced ATXN7 protein; α-tubulin was used as loading control. (D) Over-expressing the putative 3′ noncoding region of lnc-SCA7 (*lnc-SCA7-WT*, dark blue), full length lnc-SCA7 (*lnc-SCA7-FULL*, blue) and recombinant *lnc-SCA7-STOP* (light blue) in N2A cells each led to significantly increased *Atxn7* levels (dark red, red and pink, respectively) relative to control (white). (E) Over-expression of *lnc-SCA7-WT* increased ATXN7 protein; α-tubulin was used as loading control. Error bars in panels C and D, s.d.m. (*n = 3* cell cultures per condition). ** $p < 0.01$; *** $p < 0.001$; Two-tailed Student's t-test.

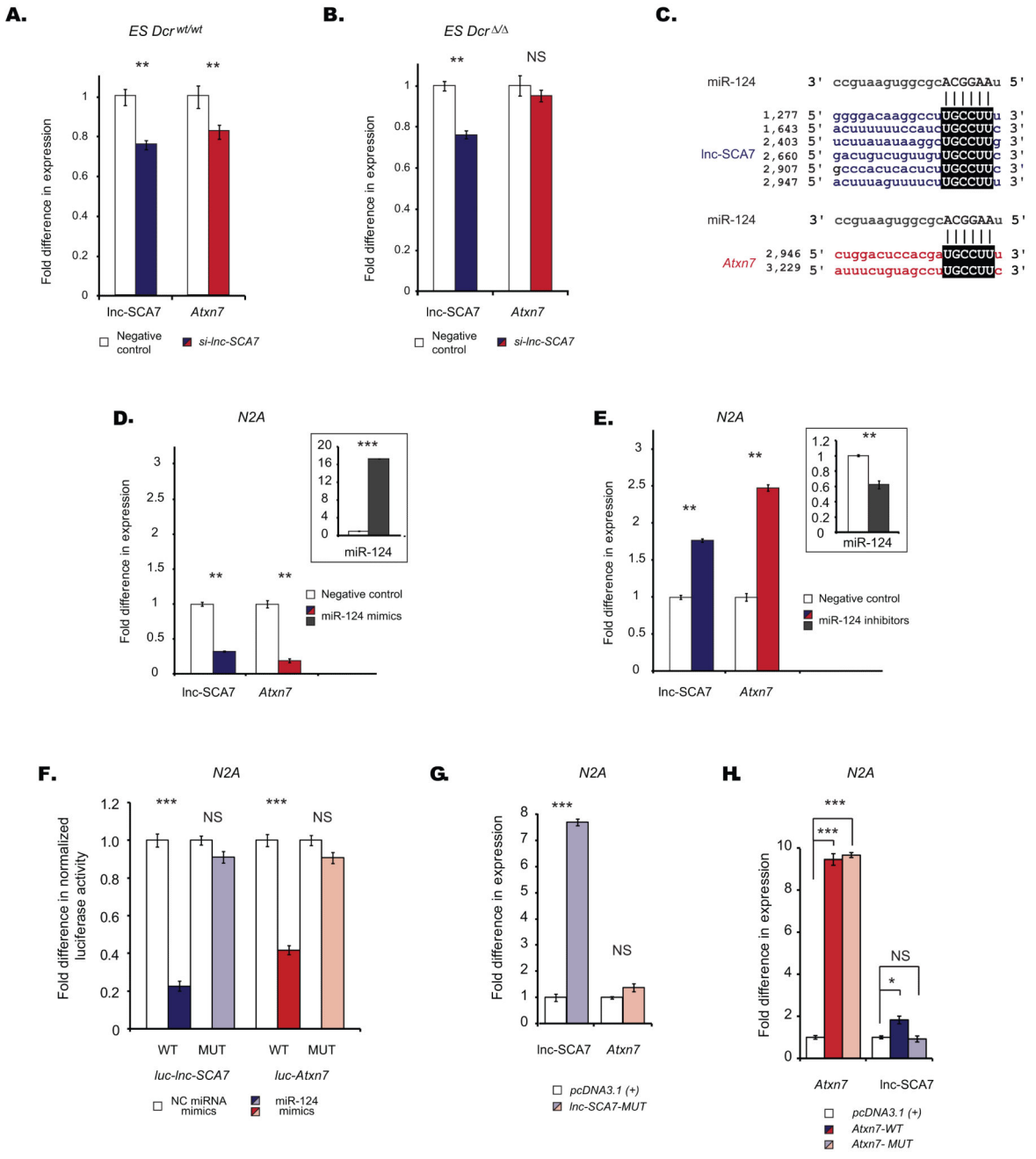

Figure 2. Post-transcriptional regulation by lnc-SCA7 is miR-124-mediated

Effect of lnc-SCA7's (blue) knock-down, using *si-lnc-SCA7*, on *Atxn7*'s abundance (red) in wild-type (DTCM/D49 XY) (A) and *Dcr-null* ($Dcr^{\Delta/\Delta}$) (B) mouse embryonic stem cells relative to control (white). (C) Pairwise alignment between miR-124 and its miRNA response elements (MREs) within the 3′ UTRs of mouse *lnc-SCA7* (top panels) or *Atxn7* (bottom panels). The initial base of the predicted binding sites in these transcripts is noted to the left of the alignment. Consecutive identical nucleotides between miR-124 seed within lnc-SCA7 and *Atxn7* are denoted by vertical lines. Difference, relative to control (white) in

lnc-SCA7 (blue) and *Atxn7*'s (red) abundance after transfection in N2As of miR-124 mimics (D) or inhibitors (E); miR-124 levels are represented in the top-right insert (dark grey). (F) Difference, relative to control (NC, white), in luciferase activity following co-transfection, in N2As, of miR-124 mimics and *luc-lnc-SCA7-WT* (blue), *luc-Atxn7- WT* (red),*luc-lnc-SCA7-MUT* (light blue) or *luc-Atxn7-MUT* (pink). G) Changes in *Atxn7* abundance (pink) following over-expression, in N2As, of *lnc-SCA7-MUT* (light blue), relative to control (white). (H) Changes in lnc-SCA7 abundance following over-expression of *Atxn7-WT* (blue) or of *Atxn7-MUT* (light blue), relative to control (white). Error bars in panels A,B, D-H, s.d.m. ($n = 3$ cell cultures per condition). ** $p < 0.01$; *** $p < 0.001$; NS $p>0.05$; Two-tailed Student's t-test.

Europe PMC Funders Author Manuscripts

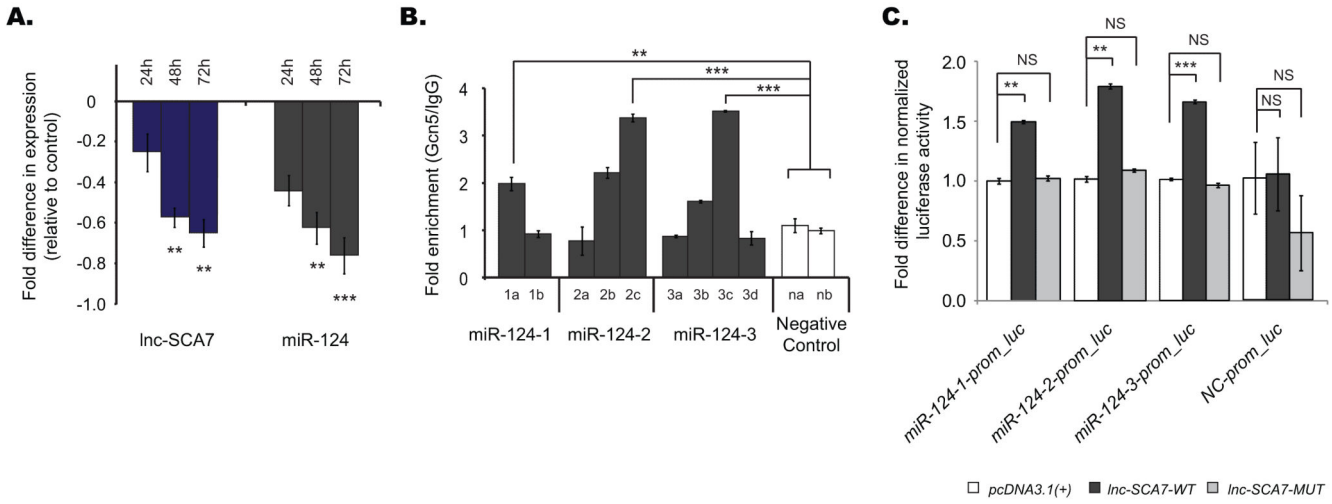

Figure 3. Transcription of miR-124 precursors is STAGA-dependent

(A) Effect in mature miR-124 levels (dark grey) of lnc-SCA7's (blue) knockdown in N2As over a 72 hour time-course. (B) Fold enrichment in Gcn5 binding, relative to IgG control, in the promoter regions of *pri-miR-124s* (dark grey; Negative control, NC, white) measured using ChIP-qPCR. (C) Fold difference in normalized luciferase activity following co-transfection of empty *pcDNA3.1(+)* (control, white), *lnc-SCA7-WT* (dark grey) or *lnc-SCA7-MUT* (light grey) with all 3 *miR-124-prom-luc* reporter constructs. Error bars s.d.m. (*n = 3* cell cultures per condition). ** $p < 0.01$; *** $p < 0.001$; NS $p>0.05$; Two-tailed Student's t-test.

Europe PMC Funders Author Manuscripts

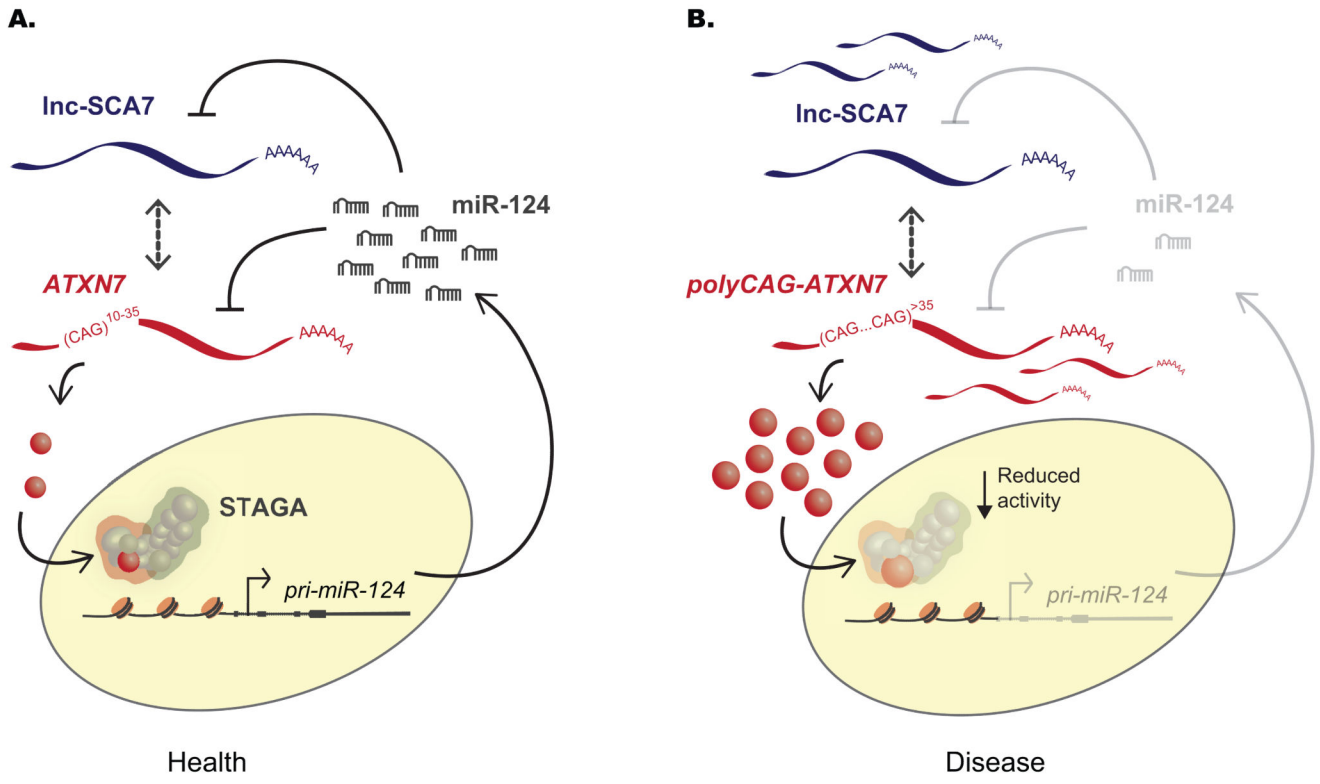

Figure 4. Crosstalking noncoding RNAs contribute to specific neurodegeneration in SCA7

(A) miR-124 (dark grey) post-transcriptionally represses and mediates crosstalk (dashed arrows) between *ATXN7* (red) and *lnc-SCA7* (blue) transcripts. STAGA co-activates transcription of miR-124 precursors. Red circles represent ATXN7 protein. (B) In SCA7, incorporation of mutant polyQ-ATXN7 into STAGA reduces its activity, decreases miR-124 abundance (light grey) and post-transcriptionally de-represses the miRNA's targets.

Europe PMC Funders Author Manuscripts

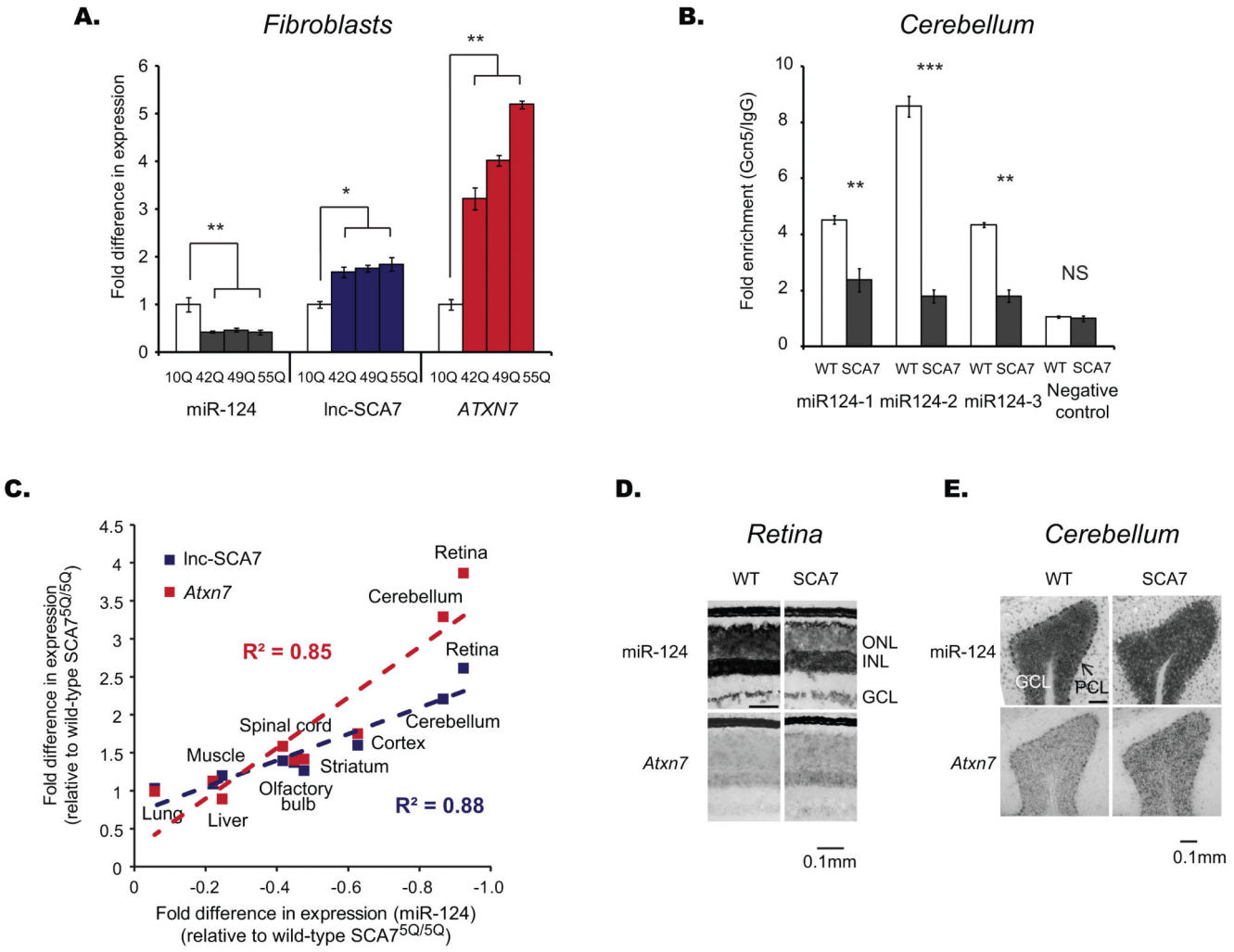

Figure 5. Contribution of noncoding RNAs to the tissue-specific pathology of SCA7

(A) Fold difference in expression of mature miR-124 abundance (dark grey), lnc-SCA7 (blue) and *ATXN7* (red) in SCA7 patient fibroblasts with 42, 49, or 55 expanded ATXN7 polyQ repeats relative to healthy control (white). (B) ChIP-qPCR revealed significantly decreased enrichment, relative to IgG control, in GCN5 binding at miR-124 promoters in $SCA7^{100Q/100Q}$ mice (dark grey) relative to control animals (white). (C) Correlation between the fold difference in expression levels between *lnc-SCA7* (Y-axis, blue) and *Atxn7* (y-axis, red) with miR-124 (x-axis) in $SCA7^{266Q/5Q}$ mice as measured using qRT-PCR and relative to matched controls, $SCA7^{5Q/5Q}$. (D and E) RNA in-situ hybridization of miR-124 and *Atxn7* in the retina and cerebellum of $SCA7^{266Q/5Q}$ mice and littermate $SCA7^{5Q/5Q}$ controls in the retina (D; ganglion cell layer (GCL), inner nuclear layer (INL), outer nuclear layer (ONL)) and cerebellum (E; granule cell layer (GCL), Purkinje cell layer (PCL)). Error bars s.d.m. for 3 cell cultures per condition (A) and cerebellum tissues derived from 3 individual mice per condition (B). ** $p < 0.01$; *** $p < 0.001$; NS $p>0.05$; Two-tailed Student's t-test $n = 3$ biological replicates per condition). Error bars represent s.d.m. **, $p < 0.01$; ***, $p < 0.001$; Student's t-test.